Original Article

Spectral computed tomography iodine concentration spatial distribution and multi-parameter quantitative analysis in the differential diagnosis of central small cell lung cancer from squamous cell carcinoma

Jiawei He[1,2], Sheng Mao[2], Hu Yuan[2], Xuan Zhou[3], Longsheng Wang[1], Chen Xue[4]^

[1]Department of Radiology, Second Affiliated Hospital of Anhui Medical University, Hefei, China; [2]Department of Radiology, The Second People's Hospital of Hefei (Hefei Hospital Affiliated to Anhui Medical University), Hefei, China; [3]Department of Respiratory, The Second People's Hospital of Hefei (Hefei Hospital Affiliated to Anhui Medical University), Hefei, China; [4]Department of Radiology, the Affiliated Brain Hospital of Nanjing Medical University, Nanjing, China

Contributions: (I) Conception and design: J He, L Wang, C Xue; (II) Administrative support: J He; (III) Provision of study materials or patients: J He, S Mao, H Yuan, X Zhou; (IV) Collection and assembly of data: J He; (V) Data analysis and interpretation: J He, L Wang, C Xue; (VI) Manuscript writing: All authors; (VII) Final approval of manuscript: All authors.

Correspondence to: Longsheng Wang, MD. Department of Radiology, Second Affiliated Hospital of Anhui Medical University, No. 678 Furong Road, Hefei Economic Development Zone, Hefei 230011, China. Email: 2639795534@qq.com; Chen Xue, MD. Department of Radiology, the Affiliated Brain Hospital of Nanjing Medical University, No. 264 Guangzhou Road, Gulou District, Nanjing 210029, China. Email: chenxue1994@njmu.edu.cn.

Background: Central small cell lung cancer (SCLC) and squamous cell carcinoma (SCC) are distinct types of lung cancer that require different treatment approaches and have varying prognoses. Accurate differentiation is crucial for clinical decision-making. However, traditional computed tomography (CT) may face challenges when their imaging features overlap. Spectral CT provides additional spectral images, offering more objective information for differentiation. This study investigated the application values of iodine concentration spatial distribution and multi-parameter quantitative analysis using a novel double-layer detector energy spectrum CT in the differential diagnosis of SCLC and SCC.

Methods: Sixty-six patients with central lung cancer (including 31 patients with SCLC and 35 patients with SCC) were examined with CT spectral imaging during arterial phase (AP) and venous phase (VP). The mean iodine concentration (IC), mean effective atomic number (Eff-Z), normalized iodine concentration (NIC), normalized iodine concentration in the proximal region (NICpro), normalized iodine concentration in the distal region (NICdis), and the differences in NIC between the proximal and distal regions in the AP and VP were calculated. The differences in parameters between central SCLC and SCC were compared, and receiver operating characteristic (ROC) curves were generated to explore the value of these parameters in distinguishing between central SCLC and SCC.

Results: The Eff-Z, IC, and NIC of SCLC were higher than SCC in the AP and VP. In terms of the spatial distribution differences in iodine concentration, both NICpro and NICdis during AP and VP were higher in SCLC compared to SCC. Moreover, ROC analysis showed that the NICdis in the VP had highest diagnostic performance in differentiating SCLC from SCC with an area under the receiver operating characteristic curve of 0.897, sensitivity of 96.80%, and a critical threshold of 0.175.

Conclusions: CT spectral imaging proves beneficial in diagnosing and differentiating between central SCLC and SCC, demonstrating significant clinical application value. Particularly, the spatial distribution of iodine concentration emerges as a valuable factor capable of enhancing diagnostic efficiency, showcasing undeniable potential.

^ ORCID: 0000-0002-9753-0782.

Keywords: Small cell lung cancer (SCLC); squamous cell carcinoma (SCC); spectrum computed tomography imaging (spectrum CT imaging); multi-parameter quantification; iodine concentration spatial distribution

Submitted Nov 03, 2024. Accepted for publication Mar 04, 2025. Published online Apr 25, 2025.
doi: 10.21037/tcr-24-2161
View this article at: https://dx.doi.org/10.21037/tcr-24-2161

Introduction

The global cancer statistics for 2020 indicate that lung cancer remains one of the malignancies with the highest incidence and mortality rates (1). Among them, central lung cancer refers to primary lung cancer occurring in the segmental level or higher, with small cell lung cancer (SCLC) and squamous cell carcinoma (SCC) being the predominant pathological types. SCLC exhibits a faster rate of cancer cell proliferation, a higher tendency for metastasis and spread, and a rapid progression of the disease compared to SCC (2-5). However, the central lung cancer lacks specific symptoms and signs, and the treatment approaches for central SCLC and SCC are markedly different (6,7). Therefore, it is utmost important for radiologists to be able to distinguish SCC and SCLC in a clinical setting for effective disease management and accurate prognosis.

Conventional computed tomography (CT) serves as the primary imaging modality for lung cancer, aiding in the differentiation between SCLC and SCC based on morphological differences, as well as variations in enhancement degree and enhancement patterns. However, distinguishing between SCLC and SCC can be challenging when their imaging features overlap. In contrast, spectral CT requires only a single scan, providing not only conventional CT images but also additional spectral images, offering more objective reference information for the differentiation diagnosis of SCLC and SCC (8). Previous studies showed that parameters of dual-layer spectral detector CT can well differentiate SCLC from non-small cell lung cancer (NSCLC) (9-11). Nevertheless, there were few studies using spectral CT to distinguish between SCLC and SCC, especially in analyzing differences in the spatial distribution of iodine concentration.

The present study retrospectively analyzed 66 patients with central SCLC and SCC confirmed by pathology. We aimed to explore differences in the iodine concentration spatial distribution and multi-parameter quantitative analysis in spectral CT and assess their values in the differential diagnosis of central SCLC and SCC. We present this article in accordance with the STARD reporting checklist (available at https://tcr.amegroups.com/article/view/10.21037/tcr-24-2161/rc).

Highlight box

Key findings

- This study investigated the diagnostic value of iodine concentration (IC) spatial distribution and multi-parameter quantitative analysis using spectral computed tomography (CT) to differentiate between small cell lung cancer (SCLC) and squamous cell carcinoma (SCC).
- Significant differences were found in IC and spectral parameters between SCLC and SCC, with SCLC showing higher mean IC, effective atomic number, and normalized IC (NIC) in both arterial phase and venous phase (VP).
- The NIC in the distal region (NICdis) during the VP demonstrated the highest diagnostic performance for distinguishing SCLC from SCC, with an area under the receiver operator characteristic curve of 0.897, sensitivity of 96.80%, and a critical threshold of 0.175.

What is known and what is new?

- Spectral CT is an emerging diagnostic tool providing quantitative data for lung cancer diagnosis.
- This study introduced the analysis of spatial iodine distribution differences as a novel method to differentiate central SCLC from SCC, with NICdis proving particularly effective. This manuscript highlighted the potential of iodine spatial distribution as a non-invasive diagnostic tool in lung cancer, specifically distinguishing SCLC from SCC, a crucial advancement in spectral CT applications.

What is the implication, and what should change now?

- Spectral CT, particularly NICdis, offers a new method to non-invasively differentiate between SCLC and SCC, reducing the need for invasive biopsies.
- Further validation in larger studies and clinical integration of spectral CT for improved lung cancer diagnostics.

Methods

Patients and setting

The current retrospective study included 66 patients of Han ethnicity diagnosed with central lung cancer through

pathological examination at The Second People's Hospital of Hefei from January 2021 to November 2023. Thirty-one patients with central SCLC and 35 patients with SCC were included. The study was conducted in accordance with the Declaration of Helsinki and its subsequent amendments. The study was approved by the responsible Human Participants Ethics Committee of The Second People's Hospital of Hefei (No. 2022-015) and informed consent was obtained from all individual participants.

The inclusion criteria were included: (I) tumors located in the bronchi at the segmental level or higher, confirmed by bronchoscopy biopsy or surgical pathology; (II) no prior anti-tumor treatment before spectral CT scanning; (III) no pulmonary atelectasis or distinguishable pulmonary atelectasis tissue from lung cancer lesions through enhanced examination; (IV) tumors were solid masses with a maximum transverse diameter greater than 20 mm; (V) no other clinical history of tumors; (VI) complete spectral CT images obtained through spectral CT scanning. The exclusion criteria were included: (I) tumors showed clear fat degeneration or air accumulation; (II) the necrotic component of the tumor exceeded half of the tumor at the level of the maximum transverse diameter; (III) history of thoracic surgery or chest trauma; (IV) inability to differentiate between SCLC tumors and metastatic lymph nodes in the pulmonary hilum region.

CT data acquisition

Triple-phase CT (i.e., unenhanced and two-phase contrast-enhanced CT examinations) was performed using Philips Healthcare IQon Spectral CT (Philips, Best, Netherlands). All patients underwent imaging craniocaudally in the supine position. The field of vision ranges from apex to diaphragm level. Patients were injected with a dose of 1.0 mL/kg non-ionic contrast medium (iodixanol, 320 mg/mL) via antecubital venous access at a rate of 3.5 mL/s during both arterial phase (AP) and venous phase (VP). The AP was started at 30 s after contrast agent injection, and VP was performed at 60 s after contrast agent injection. Parameters included tube voltages of 120 kVp, spectral CT adaptive current (140–250 mA), collimator width of 64 mm × 0.625 mm, pitch of 0.984, rotation time of 0.5 s, and matrix of 512×512. After the scans were completed, the data obtained in the enhanced double phases were reconstructed by projected spatial-spectral reconstruction (spectral, level 3). The image reconstruction image thickness was 1 mm, and the image spacing was 1 mm.

Imaging analysis

The images were analyzed using the IQon CT post-processing workstation (IntelliSpace Portal 10, Philips Healthcare). Three consecutive image sections containing the maximum cross section of the tumor and the adjacent upper and lower levels were chosen for measurement. The region of interest (ROI) was placed on solid regions of the tumor, avoiding areas with vessels, calcification, cystic, and necrotic change. Two radiologists sketched the ROI on the enhanced images, and the spectral parameters, including the iodine concentration (IC) and mean effective atomic number (Eff-Z) of the tumor were evaluated. In the comparison interface, copy/paste functions were used to ensure the consistency of the size, shape, and position of the ROIs. In addition, On the axial maximum image, the tumor was divided into three equal parts. The one-third region closest to the hilum was defined as the proximal region (PRO), and the one-third region closest to the chest wall was defined as the distal region (DIS). The measures lung cancer are as follows: (I) average Eff-Z = (Eff-Zpro + Eff-Zdis)/2; (II) average IC = (ICpro + ICdis)/2; (III) normalized iodine concentration (NIC) = focal IC/iodine concentration in aorta (ICao), average NIC in proximal region (NICpro) = ICpro/ICao, mean NIC in the distal region (NICdis) = ICdis/ICao, mean NIC in lung cancer = (NICpro + NICdis)/2, the NIC difference (differences in NIC between the proximal and the distal regions, dNIC) = NICpro – NICdis (*Figures 1*,*2*). All data were processed and analyzed by two radiologists with more than 10 years of chest CT diagnosis experience. They were blinded to any patient's clinical data to mitigating potential cognitive biases, and the mean value of the measured values of the two physicians was adopted for the final comprehensive evaluation.

Histochemical examination

All pathological diagnoses were made based on tissue samples obtained through bronchoscopy-guided biopsy or surgery. Tumor specimens underwent analysis by a pathologist with 10 years of experience in immunohistochemical staining. Unaware of clinical information and spectral CT results, the pathologist systematically numbered and assessed all sections, carefully analyzing and recording their respective pathological types. The diagnostic criteria adhered to the guidelines outlined in the World Health Organization Classification of Lung Tumors (12).

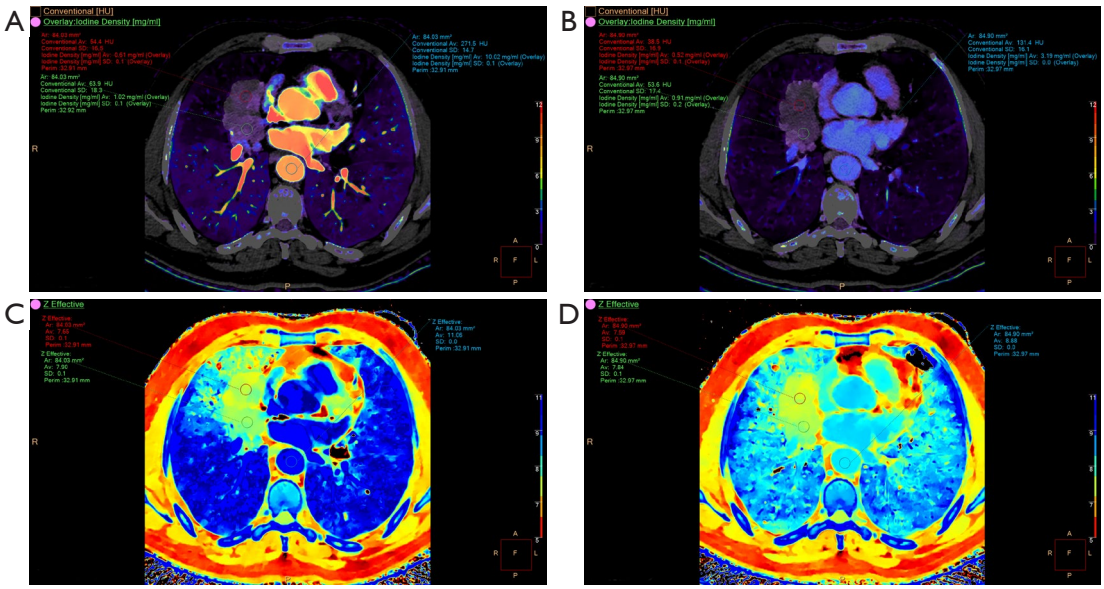

Figure 1 A 72-year-old male with squamous cell carcinoma. (A) Iodine concentration fused with conventional CT image in arterial phase; (B) iodine concentration fused with conventional CT image in venous phase; (C) Eff-Z map in arterial phase; (D) Eff-Z map in venous phase. CT, computed tomography; Eff-Z, mean effective atomic number.

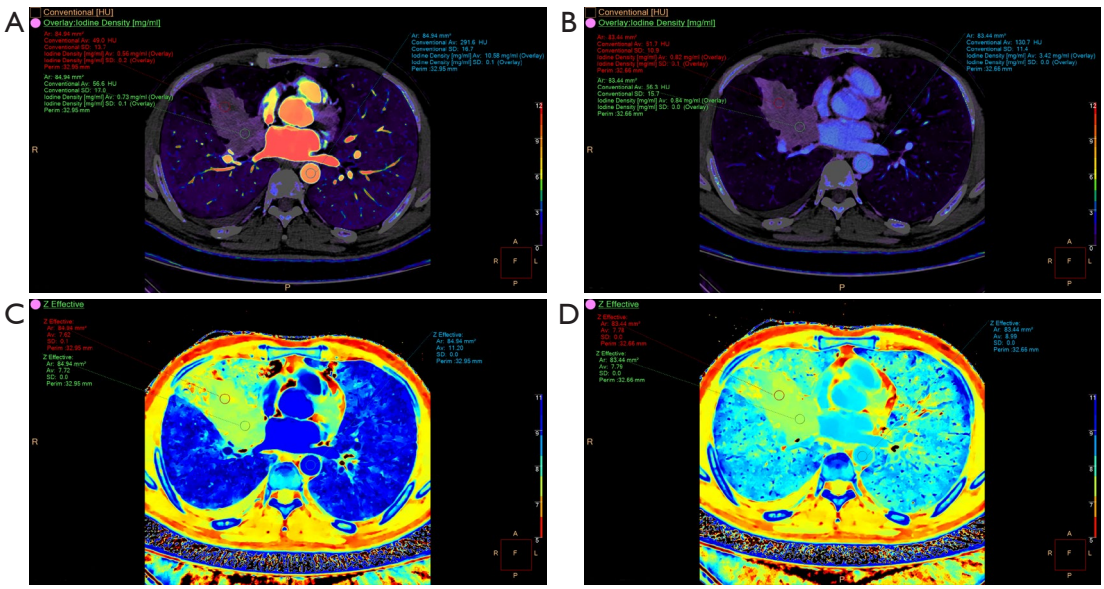

Figure 2 A 52-year-old male with small cell lung cancer. (A) Iodine concentration fused with conventional CT image in arterial phase; (B) iodine concentration fused with conventional CT image in venous phase; (C) Eff-Z map in arterial phase; (D) Eff-Z map in venous phase. CT, computed tomography; Eff-Z, mean effective atomic number.

Statistical analysis

Demographic data were analyzed using SPSS 22.0 (Chicago, IL, USA). The normal distribution of all measured data was tested by the Shapiro-Wilk test. Measurements that follow a normal distribution were expressed as mean (standard deviation). In addition, the counting data were expressed by n (%). Independent sample *t*-test was used for continuous

Table 1 Clinical characteristics of SCLC and SCC

Variable	SCLC	SCC	Statistic	P value
No. of patients	31	35		
Age (years), mean ± SD			0.507	0.61
All	71.71±8.16	70.48±11.02		
Female	70.57±8.42	58.00±1.73		
Male	72.04±8.24	71.66±10.79		
Sex, n (%)			1.538	0.21
Female	7 (22.6)	3 (8.6)		
Male	24 (77.4)	32 (91.4)		

SCC, squamous cell carcinoma; SD, standard deviation; SCLC, small cell lung cancer.

Table 2 Comparison of quantitative parameters in AP and VP of central SCC and SCLC

Group	SCLC	SCC	*t*	P
AP group				
IC (mg/mL)	1.00±0.36	0.65±0.31	4.229	<0.001
NIC (mg/mL)	0.14±0.13	0.07±0.03	2.847	0.008
Eff-Z	7.89±0.17	7.67±0.20	4.468	<0.001
VP group				
IC (mg/mL)	1.27±0.39	0.72±0.34	6.097	<0.001
NIC (mg/mL)	0.30±0.10	0.17±0.08	5.648	<0.001
Eff-Z	8.01±0.22	7.71±0.23	5.512	<0.001

Numbers are given as mean ± standard deviation unless stated otherwise. AP, arterial phase; Eff-Z, mean effective atomic number; IC, iodine concentration; NIC, normalized iodine concentration; SCC, squamous cell carcinoma; SCLC, small cell lung cancer; VP, venous phase.

variables, and chi-square test was used for counting data. A P value <0.05 was considered statistically significant. The two-sample *t*-test was performed to compare the quantitative parameters of Eff-Z, IC, NIC, NICpro, NICdis, and dNIC in the AP and VP between SCLC and SCC, with P<0.05 indicating statistical significance.

Based on the statistically significant values from the two-sample comparison, receiver operating characteristic (ROC) curve analysis was performed in SPSS to assess the diagnostic efficacy for SCLC and SCC, and calculate the cut-off value, sensitivity, and specificity in the maximal Youden index. Delong test was used to compare area under the curve (AUC), with P<0.05 was considered statistically significant.

Table 3 Comparison of iodine concentration spatial distribution in AP and VP of central SCC and SCLC

Group	SCLC	SCC	*t*	P
AP group				
NICpro (mg/mL)	0.12±0.14	0.07±0.04	1.733	0.08
NICdis (mg/mL)	0.12±0.13	0.06±0.03	2.477	0.01
dNIC (mg/mL)	0.00±0.02	0.01±0.03	–2.635	0.01
VP group				
NICpro (mg/mL)	0.29±0.10	0.20±0.10	3.831	<0.001
NICdis (mg/mL)	0.32±0.11	0.15±0.08	6.915	<0.001
dNIC (mg/mL)	0.01±0.05	0.04±0.08	–2.004	0.049

Numbers are given as mean ± standard deviation unless stated otherwise. dNIC = NICpro – NICdis. AP, arterial phase; NICdis, normalized iodine concentration in the distal region; NICpro, normalized iodine concentration in the proximal region; SCC, squamous cell carcinoma; SCLC, small cell lung cancer; VP, venous phase.

Results

Patients' information

As *Table 1* showed, the 31 patients with central SCLC (24 males, 7 females; age 71.71±8.16 years) and 35 patients with SCC (32 males, 3 females; age 70.48±11.02 years) were included in the present study. There were no significant differences in age and sex between SCLC and SCC groups (P>0.05).

Quantitative image analysis

In the multi-parameter quantification analysis, the SCLC group exhibited significantly higher values for IC, NIC, and Eff-Z in both AP and VP compared to the SCC group, with the distinction being particularly pronounced in the VP (P<0.05) (*Table 2*).

Regarding the spatial distribution of iodine concentration, the SCLC group demonstrated significantly higher values for NICdis in the AP, as well as NICpro, and NICdis in the VP, when compared to the SCC group. The SCLC group exhibited significantly lower values for dNIC in the AP and VP than the SCC group (P<0.05) (*Table 3*).

Diagnostic implication

ROC analysis was conducted to evaluate the discriminative performance of altered parameters in distinguishing

Table 4 Parameters in distinguishing the SCLC and SCC in the receiver operating characteristic analysis

Parameters	Youden Index	Threshold	Sensibility (%) (95% CI)	Specificity (%) (95% CI)	AUC (95% CI)
Eff-Zap	0.485	7.785	74.20 (59.30–88.50)	74.30 (59.40–88.10)	0.791 (0.683–0.898)
Eff-Zvp	0.532	7.780	80.80 (78.00–100.00)	57.10 (45.90–78.70)	0.832 (0.736–0.928)
ICap	0.456	0.79	74.20 (57.10–89.10)	71.40 (56.70–85.50)	0.776 (0.664–0.889)
ICvp	0.535	0.80	93.50 (83.80–100.00)	60.00 (43.80–76.10)	0.852 (0.764–0.940)
NICap	0.446	0.065	90.30 (78.60–100.00)	54.30 (36.90–71.40)	0.730 (0.608–0.852)
NICvp	0.491	0.29	54.80 (36.70–71.40)	94.30 (85.70–100.00)	0.838 (0.746–0.931)
NICprovp	0.341	0.295	48.40 (32.10–64.30)	85.70 (73.30–96.80)	0.726 (0.606–0.846)
NICdisap	0.439	0.065	83.90 (70.00–96.30)	60.00 (43.10–76.50)	0.721 (0.598–0.845)
NICdisvp	0.625	0.175	96.80 (89.20–100.00)	65.70 (50.00–80.90)	0.897 (0.825–0.968)

AUC, area under the curve; CI, confidence interval; Eff-Zap, mean effective atomic number in arterial phase; Eff-Zvp, mean effective atomic number in venous phase; ICap, iodine concentration in arterial phase; ICvp, iodine concentration in venous phase; NICap, normalized iodine concentration in arterial phase; NICdisap, normalized iodine concentration in the distal region in arterial phase; NICdisvp, normalized iodine concentration in the distal region in venous phase; NICprovp, normalized iodine concentration in the proximal region in venous phase; NICvp, normalized iodine concentration in venous phase; SCC, squamous cell carcinoma; SCLC, small cell lung cancer.

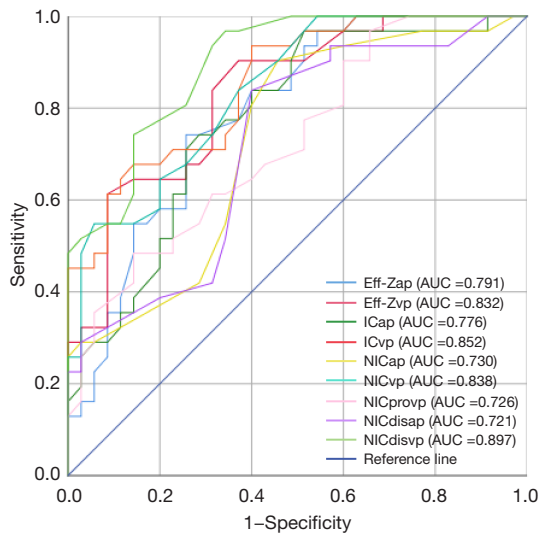

Figure 3 ROC curves for quantitative parameters in spectral CT were used to identify the small cell lung cancer and squamous cell carcinoma. AUC, area under the curve; CT, computed tomography; Eff-Zap, mean effective atomic number in arterial phase; Eff-Zvp, mean effective atomic number in venous phase; ICap, iodine concentration in arterial phase; ICvp, iodine concentration in venous phase; NICap, normalized iodine concentration in arterial phase; NICdisap, normalized iodine concentration in the distal region in arterial phase; NICdisvp, normalized iodine concentration in the distal region in venous phase; NICprovp, normalized iodine concentration in the proximal region in venous phase; NICvp, normalized iodine concentration in venous phase; ROC, receiver operating characteristic curve.

between SCLC and SCC (*Table 4* and *Figure 3*). Among these parameters, NICdis in the VP demonstrated the highest diagnostic efficacy, boasting an AUC value of 0.897, a sensitivity of 96.80%, a specificity of 65.70%, a Youden index of 0.625, and a threshold of 0.175. Following was IC in the VP, with an AUC value of 0.852, a sensitivity of 93.50%, a specificity of 60.00%, a Youden index of 0.535, and a threshold of 0.80. The Delong test revealed a significant difference in the AUC value of NICdis in the VP compared to the other parameters ($P<0.05$). The AUC values among NIC, NICpro, and NICdis during the VP were all statistically significant ($P<0.05$).

Discussion

To the best of our knowledge, this study represented the first comprehensive analysis of the spatial distribution differences in iodine concentration and multi-parameter quantitative analysis between SCLC and SCC. The results indicated distinct variations in iodine concentration spatial distribution and multi-parameter quantification between SCLC and SCC. Notably, the parameter NICdis derived from iodine concentration spatial distribution proves particularly effective in distinguishing between SCLC and SCC.

The diagnostic gold standard for lung cancer is pathological diagnosis, commonly achieved through preoperative biopsy pathology, which inevitably causes a certain degree of trauma to the human body. CT imaging is

a commonly used non-invasive method in clinical practice for the diagnosis of lung cancer. Traditional morphological spiral CT imaging from the past has lagged behind modern dynamic molecular functional imaging. Spectral CT is an innovative CT examination technique that provides more quantitative spectral information images, such as effective atomic number, iodine density map, spectral curves, etc. It, utilizing dual-layer detectors, achieves complete matching of time and spatial resolution between high and low-energy X-rays during the examination. This ensures the accuracy of the data, allowing physicians to perform immediate retrospective analysis and quantitative diagnosis through spectral parameters such as iodine values (13-15). In recent years, multiple studies have shown some progress in the field of lung cancer research using multi-parameter imaging with spectral CT (16-19). However, research on utilizing the spatial distribution differences in iodine concentration for identifying and analyzing lung cancer is rare.

In a study on anti-cancer treatment involving the uptake of nanoparticles in tumor cells, it was observed that there are metabolic activity differences of spatial distribution in tumor cells (20). A study of ^{18}F-fluorodeoxyglucose (FDG) also demonstrated significant differences in the metabolic activity of proximal and distal cells in malignant lesions (21). This indicates a notable spatial distribution variation in the metabolism of malignant tumor cells, reveal that further research can be conducted using iodine concentration parameters. Iodine density maps can visually and accurately analyze and quantify the iodine uptake in tissues and organs, reflecting the metabolic and blood flow changes associated with lesions (22). The iodine content of tumors primarily depends on two factors: microvascular density and the amount of iodine infiltrating into the intercellular space. The IC value can quantify the blood supply to tumor tissues but is susceptible to factors such as contrast agent flow rate and concentration, the dose of injected contrast agent, patient metabolism, and cardiac output. NIC can reduce the impact of individual differences on tumor iodine content, providing more accurate and reliable results (8,23).

In the current study, the mean values of IC, NIC, and dNIC for solid components in both proximal and distal regions of SCLC and SCC were assessed to evaluate their internal hemodynamic changes. The results showed that the average IC and NIC in SCLC were significantly higher than SCC, particularly in the VP. It is speculated to be attributed to the comparable microvascular density in both SCLC and SCC. However, in the case of SCLC, it is mainly composed of immature capillaries, leading to an imperfect basement membrane, increased permeability, and consequently, a higher iodine uptake in the intercellular space compared to SCC (24). Furthermore, the Eff-Z reaction reflects the material composition with higher sensitivity than HU attenuation. It can accurately analyze tissue information with small CT value differences, and it is quantified in color (15,25). Eff-Z can also indirectly show the accumulation of contrast agents in tissues and diagnose tumor pathology subtypes (26,27). In the present study, the mean values of Eff-Z during both AP and VP were higher in the proximal and distal regions of SCLC compared to SCC. This observation was related to the internal tissue structure, growth patterns, and blood supply conditions of the two lung cancer pathologies. Currently, there was limited research on Eff-Z in lung tumors, warranting further exploration of its application value.

In terms of diagnostic efficacy, the current study demonstrated that the diagnostic performance of various parameters is generally higher during the VP. Among them, NICdis in the VP exhibited the best diagnostic performance, with an AUC value of 0.897, sensitivity of 96.80%, and specificity of 65.70%. Following closely was IC in the VP, with an AUC value of 0.852, sensitivity of 93.50%, and specificity of 60.00%. Through the Delong test, the statistically significant differences in AUC among spectral CT parameters were mainly in the VP. Among them, the diagnostic performance of the NICdis in the VP was particularly excellent, which was consistent with previous studies (9,19). Mu *et al.* demonstrated that the normalized iodine density in the VP exhibited optimal diagnostic performance in differentiating SCLC from non-SCLC, with the AUC of 0.917, a sensitivity of 92.9%, and a specificity of 80% (9). Additionally, previous literature showed that when distinguishing SCC from adenocarcinoma using the ROC curve, the slope of the spectral curve in the VP stands out with the highest diagnostic performance, boasting an AUC of 0.864, a sensitivity of 85.8%, and a specificity of 74.3% (19). All of these indicated the high diagnostic efficiency in the VP for lung cancer. In the current study, reasons for the best diagnostic efficacy of the VP, especially NICdis in the VP, in differentiating SCLC and SCC were as follows: firstly, malignant tumors often exhibit disorganized and tortuous microvascular arrangements, with the contrast agent moving slowly within the vessels. It is only in the VP that the microvasculature can be fully filled with the contrast agent (28). Secondly, the blood supply to malignant tumors is predominantly from the bronchial arteries, and the lymphatic and venous drainage systems are either absent or

underdeveloped, leading to impaired iodine contrast agent reflux (29). This results in a prolonged plateau phase. The microvascular types of SCLC and SCC differ, as do their lymphatic and venous drainage systems (24). These factors cause differences in iodine content per unit tumor volume, which is most pronounced in the VP, making the venous phase the optimal period for calculating tumor iodine content. Thirdly, SCC features tightly packed cancerous tissue, often forming keratin pearls, cancer nests, and special intercellular bridge structures. The tumor cells exhibit a piling growth pattern, with relatively slow growth and poor blood supply (30,31). In contrast, SCLC has sparse cytoplasm, a large nuclear-to-cytoplasmic ratio, loose structure, and diffuse growth with a higher proportion of stromal fibers (32-34). Due to the substantial difference in the proportion of parenchyma and stroma between SCC and SCLC, the dispersion rate of iodine contrast agent within the tumor varies, and the spatial distribution within the tumor also differs. Tumor tissue located distally, farther from the main blood supply from the bronchial arteries, exhibits a greater metabolic activity difference. Additionally, NIC can reduce individual differences in the calculation of iodine content. These factors collectively explain why the VP and NICdisvp offer the best diagnostic efficacy. The findings revealed certain differences in the iodine concentration spatial distribution and multiple quantitative parameters in spectral CT between SCLC and SCC, which was helpful for their differential diagnosis.

Limitation and future perspectives

The main limitations of this study were as follows: Firstly, the sample size was relatively small, which may introduce selection bias. Secondly, the study exhibited gender data imbalance, likely due to variations in lung cancer incidence across genders. Thirdly, the differentiation degree of lung cancer was not further subdivided. Additionally, for central SCLC and SCC, most were discovered with relatively large volumes. The measurement of ROI was based on the maximum level, rather than considering the three-dimensional volume of the tumor mass in the proximal and distal regions. Finally, as a retrospective study, the results may be subject to inherent biases related to this design. The lack of external validation also limited the generalizability of the findings. In the future, we will further investigate and address these limitations. We plan to continue expanding the sample size and use a multi-center prospective cohort study to validate the diagnostic potential of spectral CT parameters, ensuring the broad applicability of the results. Additionally, we will explore whether spectral CT parameters can predict treatment response or patient prognosis. At the same time, exploring the application of artificial intelligence technology for more precise and standardized analysis will be a key step in enhancing the robustness and clinical relevance of these findings.

Conclusions

In conclusion, the utilization of multi-parameter quantitative analysis (IC, NIC, Eff-Z) and the iodine concentration spatial distribution (NICpro, NICdis, dNIC) differences in spectral CT offered a novel potential approach for distinguishing SCLC from SCC. Particularly, the spatial distribution of iodine concentration emerges as a valuable factor capable of enhancing diagnostic efficiency, showcasing undeniable potential.

Acknowledgments

None.

Footnote

Reporting Checklist: The authors have completed the STARD reporting checklist. Available at https://tcr.amegroups.com/article/view/10.21037/tcr-24-2161/rc

Data Sharing Statement: Available at https://tcr.amegroups.com/article/view/10.21037/tcr-24-2161/dss

Peer Review File: Available at https://tcr.amegroups.com/article/view/10.21037/tcr-24-2161/prf

Funding: This study was supported by the clinical medicine discipline construction project of Anhui Medical University (No. 2021lcxk029); Research Projects of The Second People's Hospital of Hefei (No. 2022yyb013).

Conflicts of Interest: All authors have completed the ICMJE uniform disclosure form (available at https://tcr.amegroups.com/article/view/10.21037/tcr-24-2161/coif). The authors have no conflicts of interest to declare.

Ethical Statement: The authors are accountable for all aspects of the work in ensuring that questions related to the accuracy or integrity of any part of the work are

appropriately investigated and resolved. The study was conducted in accordance with the Declaration of Helsinki and its subsequent amendments. The study was approved by the responsible Human Participants Ethics Committee of The Second People's Hospital of Hefei (No. 2022-015) and informed consent was obtained from all individual participants.

References

1. Sung H, Ferlay J, Siegel RL, et al. Global Cancer Statistics 2020: GLOBOCAN Estimates of Incidence and Mortality Worldwide for 36 Cancers in 185 Countries. CA Cancer J Clin 2021;71:209-49.
2. Xu X, Sui X, Zhong W, et al. Clinical utility of quantitative dual-energy CT iodine maps and CT morphological features in distinguishing small-cell from non-small-cell lung cancer. Clin Radiol 2019;74:268-77.
3. Nicholson AG, Chansky K, Crowley J, et al. The International Association for the Study of Lung Cancer Lung Cancer Staging Project: Proposals for the Revision of the Clinical and Pathologic Staging of Small Cell Lung Cancer in the Forthcoming Eighth Edition of the TNM Classification for Lung Cancer. J Thorac Oncol 2016;11:300-11.
4. Sen T, Takahashi N, Chakraborty S, et al. Emerging advances in defining the molecular and therapeutic landscape of small-cell lung cancer. Nat Rev Clin Oncol 2024;21:610-27.
5. Zhang C, Wang K, Wang H. The emerging landscape and future perspective of SCLC transformation: From molecular mechanisms to therapeutic strategies. Crit Rev Oncol Hematol 2025;207:104616.
6. Akopov A, Papayan G. Photodynamic theranostics of central lung cancer: Present state and future prospects. Photodiagnosis Photodyn Ther 2021;33:102203.
7. Zhang X, Fu Z, Gong G, et al. Implementation of diffusion-weighted magnetic resonance imaging in target delineation of central lung cancer accompanied with atelectasis in precision radiotherapy. Oncol Lett 2017;14:2677-82.
8. Wu F, Zhou H, Li F, et al. Spectral CT Imaging of Lung Cancer: Quantitative Analysis of Spectral Parameters and Their Correlation with Tumor Characteristics. Acad Radiol 2018;25:1398-404.
9. Mu R, Meng Z, Zhang X, et al. Parameters of Dual-layer Spectral Detector CT Could be Used to Differentiate Non-Small Cell Lung Cancer from Small Cell Lung Cancer. Curr Med Imaging 2022;18:1070-8.
10. Wen Q, Yue Y, Shang J, et al. The application of dual-layer spectral detector computed tomography in solitary pulmonary nodule identification. Quant Imaging Med Surg 2021;11:521-32.
11. Ma X, Xu M, Tian XJ, et al. A Retrospectively Study: Diagnosis of Pathological Types of Malignant Lung Tumors by Dual-layer Detector Spectral Computed Tomography. Technol Cancer Res Treat 2022;21:15330338221074498.
12. Nicholson AG, Tsao MS, Beasley MB, et al. The 2021 WHO Classification of Lung Tumors: Impact of Advances Since 2015. J Thorac Oncol 2022;17:362-87.
13. Greffier J, Villani N, Defez D, et al. Spectral CT imaging: Technical principles of dual-energy CT and multi-energy photon-counting CT. Diagn Interv Imaging 2023;104:167-77.
14. Hickethier T, Wenning J, Bratke G, et al. Evaluation of soft-plaque stenoses in coronary artery stents using conventional and monoenergetic images: first in-vitro experience and comparison of two different dual-energy techniques. Quant Imaging Med Surg 2020;10:612-23.
15. Rassouli N, Etesami M, Dhanantwari A, et al. Detector-based spectral CT with a novel dual-layer technology: principles and applications. Insights Imaging 2017;8:589-98.
16. Mu R, Meng Z, Guo Z, et al. Dual-layer spectral detector computed tomography parameters can improve diagnostic efficiency of lung adenocarcinoma grading. Quant Imaging Med Surg 2022;12:4601-11.
17. Wen LJ, Zhao QY, Yin YH, et al. Application value of double-layer spectral detector CT in differentiating central lung cancer from atelectasis. Ann Palliat Med 2022;11:1990-6.
18. Liu BC, Ma HY, Huang J, et al. Does dual-layer spectral detector CT provide added value in predicting spread through air spaces in lung adenocarcinoma? A preliminary study. Eur Radiol 2024;34:4176-86.
19. Mu R, Meng Z, Guo Z, et al. Diagnostic value of dual-

layer spectral detector CT in differentiating lung adenocarcinoma from squamous cell carcinoma. Front Oncol 2022;12:868216.
20. Terracciano R, Carcamo-Bahena Y, Royal ALR, et al. Zonal Intratumoral Delivery of Nanoparticles Guided by Surface Functionalization. Langmuir 2022;38:13983-94.
21. Zhao L, Tong L, Lin J, et al. Characterization of solitary pulmonary nodules with 18F-FDG PET/CT relative activity distribution analysis. Eur Radiol 2015;25:1837-44.
22. Grob D, Smit E, Prince J, et al. Iodine Maps from Subtraction CT or Dual-Energy CT to Detect Pulmonary Emboli with CT Angiography: A Multiple-Observer Study. Radiology 2019;292:197-205.
23. Cheng Z, Wang Y, Yuan M, et al. CT perfusion imaging can detect residual lung tumor early after radiofrequency ablation: a preliminary animal study on both tumoral and peri-tumoral region assessment. J Thorac Dis 2022;14:64-75.
24. Birau A, Ceausu RA, Cimpean AM, et al. Assessement of angiogenesis reveals blood vessel heterogeneity in lung carcinoma. Oncol Lett 2012;4:1183-6.
25. Simard M, Bär E, Blais D, et al. Electron density and effective atomic number estimation in a maximum a posteriori framework for dual-energy computed tomography. Med Phys 2020;47:4137-49.
26. Deniffel D, Sauter A, Fingerle A, et al. Improved differentiation between primary lung cancer and pulmonary metastasis by combining dual-energy CT-derived biomarkers with conventional CT attenuation. Eur Radiol 2021;31:1002-10.
27. Kim C, Kim W, Park SJ, et al. Application of Dual-Energy Spectral Computed Tomography to Thoracic Oncology Imaging. Korean J Radiol 2020;21:838-50.
28. Zhang Z, Zou H, Yuan A, et al. A Single Enhanced Dual-Energy CT Scan May Distinguish Lung Squamous Cell Carcinoma From Adenocarcinoma During the Venous phase. Acad Radiol 2020;27:624-9.
29. Hou WS, Wu HW, Yin Y, et al. Differentiation of lung cancers from inflammatory masses with dual-energy spectral CT imaging. Acad Radiol 2015;22:337-44.
30. Neppl C, Zlobec I, Schmid RA, et al. Validation of the International Tumor Budding Consensus Conference (ITBCC) 2016 recommendation in squamous cell carcinoma of the lung-a single-center analysis of 354 cases. Mod Pathol 2020;33:802-11.
31. Mairinger T. Histology, cytology and molecular diagnostics of lung cancer. Pathologe 2019;40:649-61.
32. Travis WD, Brambilla E, Nicholson AG, et al. The 2015 World Health Organization Classification of Lung Tumors: Impact of Genetic, Clinical and Radiologic Advances Since the 2004 Classification. J Thorac Oncol 2015;10:1243-60.
33. Toyokawa G, Kozuma Y, Matsubara T, et al. Radiological Features of the Surgically Resected Small-sized Small-cell Lung Cancer on Computed Tomography. Anticancer Res 2017;37:877-81.
34. Zheng M. Classification and Pathology of Lung Cancer. Surg Oncol Clin N Am 2016;25:447-68.

Cite this article as: He J, Mao S, Yuan H, Zhou X, Wang L, Xue C. Spectral computed tomography iodine concentration spatial distribution and multi-parameter quantitative analysis in the differential diagnosis of central small cell lung cancer from squamous cell carcinoma. Transl Cancer Res 2025;14(4):2250-2259. doi: 10.21037/tcr-24-2161